New insights on the mineralization of dissolved organic matter in central, intermediate, and deep water masses of the northeast North Atlantic

X.A. Álvarez–Salgado,[a,*] M. Nieto–Cid,[a] M. Álvarez,[b] F.F. Pérez,[a] P. Morin,[c] and H. Mercier[d]

[a] Consejo Superior de Investigaciones Científicas – Instituto de Investigacións Mariñas (IIM–CSIC), Vigo, Spain

[b] Instituto Español de Oceanografía (IEO), Centro Oceanográfico de A Coruña, A Coruña, Spain

[c] Centre National de la Recherche Scientifique (CNRS), Station Biologique de Roscoff, Roscoff Cedex, France

[d] Centre National de la Recherche Scientifique (CNRS), Laboratoire de Physique des Océans, Institut Français de Recherche pour l'Exploitation de la Mer (IFREMER) Centre de Brest, Plouzané, France

* Corresponding author: xsalgado@iim.csic.es

Running head: North Atlantic dissolved organic matter

Acknowledgements

We thank all the participants in the 'Observatoire de la variabilité interannuelle et décennale en Atlantique Nord' (OVIDE) 2002 cruise and the crew of R/V *Thalassa*, for their valuable help. Support for this work came from the Spanish Ministry of Science and Technology grant REN2001–4965–E. M.A. was funded by a postdoctoral fellowship of the European Social Fund–Consejo Superior de Investigaciones Científicas I3P program. X.A.A.S. and M.A. were supported by the Spanish Ministry of Science and Innovation (Malaspina expedition, grant CSD2008–00077). F.F.P. was supported by the Spanish Ministry of Economy and Competitiveness project 'Carbon Transport and Acidification Rates in the North Atlantic' (CATARINA, grant CTM2010–17141) co–financed by the European Fund for Regional Development (FEDER). H.M. was supported by the 'Centre National de la Recherche Scientifique' (CNRS). The OVIDE project was funded by the 'Institut Français de Recherche pour l'Exploitation de la Mer' (IFREMER), the 'Centre National de la Recherche Scientifique' (CNRS), the 'Institut National des Sciences de l'Universe' (INSU), and the French National Program 'Les Enveloppes Fluides et l'Environnement' (LEFE). The comments and recommendations of two anonymous reviewers are also acknowledged

Abstract

An optimum multiparameter (OMP) analysis was applied to the samples collected during a cruise in the northeast North Atlantic with the aim of objectively defining water mass realms and calculating water mass mixing-weighted average (archetypal) concentrations of dissolved organic carbon (DOC) and nitrogen (DON) and fluorescent dissolved organic matter (FDOM). The profile of archetypal DOC—which retains the basin-scale variability from the formation area of the water masses to the study area—was modeled with a constant initial concentration of 60 ± 1 mmol kg^{-1} that decreased linearly with increasing apparent oxygen utilization (AOU) at a rate of –0.20 ± 0.03 mol C per mol of AOU. The archetypal C:N ratio of dissolved organic matter was also modeled with a constant initial molar ratio of 11.5 ± 0.4 that increased at a rate of 0.06 ± 0.01 per μmol kg^{-1} of AOU. The profile of archetypal FDOM was modeled with a constant initial humic-like fluorescence of 0.54 ± 0.07 quinine sulphate units that increased at a rate of 0.009 ±0.001 g equivalent of quinine sulphate per mol of AOU. Only the Denmark Strait Overflow Water departed from this behavior because of the marked terrestrial influence of Arctic rivers during the formation of this water mass. The variability not explained by the archetypal concentrations —which retain the local variability— suggested that N-poor DOM was mineralized in the study area, and that the efficiency of the local production of humic-like substances was directly proportional to the ventilation of the corresponding water mass realms.

Introduction

The role played by dissolved organic matter (DOM) in the metabolic balance of the ocean is still a subject of open debate (Carlson et al. 2010; Hansell et al. 2012). It is currently accepted that DOM is responsible for 10–20% of the oxygen demand in the mesopelagic ocean (200–1000 m; Arístegui et al. 2002). For the case of the bathypelagic ocean (1000 m–bottom), considering the 14 μmol C L^{-1} decrease of dissolved organic carbon (DOC) from the deep North Atlantic to the Deep North Pacific (Hansell and Carlson 1998; Hansell et al. 2009; 2012) and the 2 Kyr that North Atlantic Deep Water (NADW) needs to cover that distance (Hansell et al. 2012), it results that the global average DOC respiration rate is 7 nmol C L^{-1} yr^{-1} whereas the total respiration is 130 ± 10 nmol C L^{-1} yr^{-1} according to different oxygen utilization rate estimates (Sarmiento and Gruber 2006). Therefore, DOM represents only about 5% of the organic matter respired in the global deep ocean, where the oxygen demand would be supported almost exclusively by the flux of sinking particles (Jahnke 1996; Carlson et al. 2010; Hansell et al. 2012).

This global pattern can be dramatically altered in the intermediate and deep ocean ventilation sites, particularly in the northern North Atlantic, where the ocean's overturning circulation can inject fresh DOM below the main thermocline (Hansell and Carlson 1998; Kramer et al. 2005; Carlson et al. 2010). In fact, the average DOC respiration rate in the about 80 yr transit of the NADW from the Greenland to the Sargasso seas is about 50 nmol C L^{-1} yr^{-1} (Hansell and Carlson 1998; Hansell et al. 2012). Fresh DOM is also transported downwards to intermediate depths during the formation and circulation of North Pacific Intermediate Water (Doval and Hansell 2000; Hansell et al. 2002). In the case of the northern North Atlantic there is a scarce knowledge about the relative importance of the complex mixing pattern of water masses, which form with different preformed DOM levels, compared

with the biogeochemical transformations experienced by DOM during that mixing but *see* Carlson et al. (2010) and Hansell et al. (2012).

In the present study , we will use an optimum multiparameter (OMP) analysis of the thermohaline and chemical characteristics of the water masses that mix in the northeast North Atlantic as an objective tool to define water mass realms, water mass mixing–weighted average concentrations of dissolved organic carbon (DOC) and nitrogen (DON) and humic–like substances and the basin vs. local scale mineralization patterns of these parameters along the 'Observatoire de la variabilité interannuelle et décennale en Atlantique Nord' (OVIDE) line, which intercepts or navigates nearby to the formation area of most of the water masses that circulate in the North Atlantic.

Methods

Sampling program— The cruise OVIDE 2002 was conducted from 19 June to 11 July 2002, on board R/V *Thalassa*. Ninety one full–depth hydrographic stations were occupied, from the continental shelf off Greenland to Lisbon (Fig. 1). Salinity (S), potential temperature (θ), dissolved oxygen (O_2) nitrate (NO_3), phosphate (PO_4), and silicate (SiO_4) profiles were obtained at every station (maximum 30 levels). Dissolved organic carbon (DOC) and nitrogen (DON), and fluorescence of fluorescent dissolved organic matter (FDOM) profiles were determined at 30 stations (*see* black dots in Fig. 1) and selected depths (maximum 15 levels). Samples for dissolved organic matter analysis were collected in 10 mL precombusted glass ampoules. After acidification to pH < 2, the ampoules were heat–sealed and stored at 4ºC until DOC and total dissolved nitrogen (TDN) analysis. They were measured with a nitrogen–specific Antek 7020 nitric oxide chemiluminescence detector coupled in series with the carbon–specific Infra–red Gas Analyzer of a Shimadzu Total Organic Carbon 5000 analyzer.

The measurement error was ±0.7 μmol kg^{-1} for carbon and ±0.3 μmol kg^{-1} for nitrogen. Their respective accuracies were tested with the reference materials provided by D.A. Hansell (University of Miami), which were run once per day just after calibration with a mixed standard of potassium hydrogen phthalate and glycine. We obtained an average concentration of 44.5 ± 1.1 μmol L^{-1} of C and 21.5 ± 0.3 μmol L^{-1} of N (n = 17) for the deep ocean reference (Sargasso Sea deep water, 2600 m) minus blank reference materials. The nominal values for TOC and TDN provided by the reference laboratory are 44.0 ± 1.5 μmol C L^{-1} and 21.1–21.3 μmol N L^{-1}. Nutrient salts were determined onboard by standard segmented flow analysis with colorimetric detection. DON was obtained by subtracting NO_3 from TDN, and the error propagation of the analytical determination of both variables, ±0.1 and ±0.3 μmol kg^{-1} of N respectively, was calculated as $\sqrt{er_{NO3}{}^2 + er_{TDN}{}^2}$ = 0.32 μmol kg^{-1} of N. FDOM was determined on board at the ship lab temperature (20ºC) with a Perkin Elmer LS50 spectrofluorometer equipped with a xenon discharge lamp, equivalent to 20 kW for 8 μs duration. Slit widths were fixed to 10 nm for the excitation and emission wavelengths and the scan speed was 250 nm min^{-1}. Measurements were performed at the excitation and emission wavelengths of 320 nm and 410 nm, respectively, characteristic of marine humic–like substances absorbing in the ultraviolet C (Coble 1996). The fluorescence of ultraviolet–radiated Milli–Q at these excitation and emission wavelengths was subtracted from all samples. Factory–set excitation and emission corrections of the instruments were used. Following Coble (1996), the fluorescence intensities were expressed in quinine sulphate units (QSU) by calibrating the instrument at the excitation and emission wavelengths of 350 nm and 450 nm, respectively, against a quinine sulphate dihydrate (QS) standard made up in 0.05 mol L^{-1} sulphuric acid. The measurement error was ±0.04 QSU.

Extended optimum multi parameter (OMP) water mass analysis— The water masses present in the northeast North Atlantic have been already identified and evaluated by means of an extended OMP analysis of the World Ocean Circulation Experiment (WOCE) line A25 (Álvarez et al. 2004). The same method has been used here to obtain the proportions of the water masses that mix along the OVIDE 2002 line. Briefly, the OMP analysis consists on quantifying the proportions of the source water types (SWTs) that contribute to a given water sample. A briefing about the hydrographic characteristics, formation areas, circulation patterns and selected references about the water masses relevant for this analysis can be found in Table 1.

The mixing is solved by minimizing the residuals of the linear mixing equations for θ, S, SiO_4, O_2, NO_3, and PO_4 in a non–negative least squares sense, where mass is stringently conserved and the contributions of the different SWTs must be positive. θ, S, and SiO_4 are assumed to behave conservatively, whereas O_2, NO_3, and PO_4 are non–conservative. The set of mixing equations to be solved for a sample j is:

$$1 = \sum_i x_{ij} \tag{1}$$

$$\theta_j = \sum_i x_{ij} \cdot \theta_i \tag{2}$$

$$S_j = \sum_i x_{ij} \cdot S_i \tag{3}$$

$$SiO_{4j} = \sum_i x_{ij} \cdot SiO_{4i} \tag{4}$$

$$O_{2j} = \sum_i x_{ij} \cdot {O_{2i}}^0 - \Delta O_{2j} \tag{5}$$

$$NO_{3j} = \sum_i x_{ij} \cdot NO_{3i}{}^0 + \Delta O_{2j} / R_N \quad (6)$$

$$PO_{4j} = \sum_i x_{ij} \cdot PO_{4i}{}^0 + \Delta O_{2j} / R_P \quad (7)$$

where x_{ij} is the proportion of the SWT i in sample j; θ_j, S_j, SiO_{4j}, O_{2j}, NO_{3j}, and PO_{4j} are the thermohaline and chemical characteristics of sample j; θ_i, S_i, SiO_{4i}, $O_{2i}{}^0$, $NO_{3i}{}^0$, and $PO_{4i}{}^0$ are the thermohaline and chemical characteristic of the SWT i in its formation area; ΔO_{2j} is the oxygen anomaly of sample j due to the respiration of organic matter, which is very close to the apparent oxygen utilization (AOU) since $O_{2i}{}^0$ is assumed to be near saturation conditions; and R_N and R_P are the stoichiometric coefficients of oxygen consumption to nitrate and phosphate production during the mineralization of biogenic organic matter. The total number of samples, *n*, included in the OMP analysis was 1937.

The thermohaline and chemical characteristics of the SWTs observed along the OVIDE line were slightly adapted from the definitions of Álvarez et al. (2004) along WOCE line A25 and are shown in Table 2. The selected SWTs are eastern North Atlantic central water of 15ºC ($ENACW_{15}$), 12ºC ($ENACW_{12}$), and 8ºC ($ENACW_8$), Subarctic intermediate water (SAIW), diluted Antarctic intermediate water (AIW), Mediterranean water (MW), Labrador Sea water (LSW), Iceland–Scotland overflow water (ISOW), Denmark Strait overflow water (DSOW) and lower deep water (LDW). $ENACW_{12}$ corresponds to the mode water defined by Harvey (1982) and $ENACW_8$ to the so called subpolar mode water (SPMW). Eqs. 1 to 7 were weighted according to the variability of the thermohaline and chemical properties in the formation region and the analytical precision of each measurement (*see* row W in Table 2). A weight of 100 was set to Eq. 1, in such a way that mass was always accurately conserved. For each sample j, the system of linear mixing Eqs. 1 to 7 contains eleven unknowns (ten x_{ij}, one

for each SWT, and ΔO_{2j}), but a maximum of seven SWTs can be considered simultaneously. This inconvenience was solved assuming some reasonable vertical constraints to the water mass mixing following Álvarez et al. (2004). Initial R_N and R_P values of 10 mol O_2 mol N^{-1} and 150 mol O_2 mol P^{-1}, respectively, were tested and iterated to obtain the minimum residuals of Eqs. 1 to 7. The retained R_N and R_P values were 9.4 ± 0.3 mol O_2 mol N^{-1} and 162 ± 5 mol O_2 mol P^{-1}, respectively.

The OMP analysis has been able to reproduce with a high confidence the thermohaline and chemical fields along the OVIDE line, as indicated by the determination coefficients (R^2 > 0.985) between the measured and the predicted values of the different tracers and the low standard deviation of the corresponding residuals (SD res), which kept slightly higher than the analytical error of the measurements (Table 2).

Water mass mixing–weighted average concentrations of chemical parameters in the water masses of the northeast North Atlantic— On basis of the concentration of any chemical parameter (N) and the proportions of the 10 SWTs identified in this study, the water mass mixing–weighted average concentration of N in each SWT, hereinafter the archetypal concentration of N, was obtained as follows:

$$< N_i >= \frac{\sum_j x_{ij} \cdot N_j}{\sum_j x_{ij}} \quad (8)$$

Where $<N_i>$ is the archetypal concentration of N in SWT i; N_j is the concentration of N in sample j; and x_{ij} is the proportion of SWT i in sample j. The standard deviation (SD) of the estimated archetypal concentration of N was calculated as:

$$SD_{N_i} = \frac{\sqrt{\sum_j x_{ij} \cdot \left(N_j - < N_i >\right)^2}}{\sum_j x_{ij}} \quad (9)$$

Application of Eq. 8 to the longitude (LON), latitude (LAT), and pressure (Z) of the samples allowed the calculation of the corresponding archetypal values for each SWT (<LON_i>, <LAT_i>, and <Z_i>). These archetypal values represent the center of mass, i.e., the SWT proportion–weighted average location of each SWT.

Therefore, the archetypal concentration of N for SWT i, <N_i>, would represent the average concentration of N in the center of mass of SWT i in the study site (<LON_i>, <LAT_i>, and <Z_i>), the OVIDE 2002 line in our case. Conceptually, <N_i> would retain: the variability of N related to the conservative mixing of SWT concentrations in their formation areas, N_i^0; plus the variability related to the basin-scale mineralization processes from the formation area of each water mass to its center of mass.

Finally, the proportion of the total volume of the sampled section occupied by SWT i (<$\%VOL_i$>) was simply calculated as:

$$< \%VOL_i >= 100 \cdot \frac{\sum_j x_{ij}}{n} \quad (10)$$

Where *n*, is the number of samples, 1937 for LON, LAT, Z, O_2, NO_3, PO_4, and SiO_4, and 333 for DOC, DON, and FDOM. The values of <LON_i>, <LAT_i>, <Z_i>, and <$\%VOL_i$> for each SWT are summarized in Table 2.

Mixing model of dissolved organic matter — Once the SWT proportions of each sample (x_{ij}) has been calculated, the contribution of water mass mixing plus the basin–scale mineralization from the formation area of the water mass to their respective centers of mass along the OVIDE 2002 line to the total variability of any chemical variable (N) can be

assessed following the method proposed by Pérez et al. (1993). It consists of performing a multiple linear regression of N_j with the SWT proportions (x_{ij}) calculated in the previous section. A system of n linear equations (one per sample) with 10 coefficients (one per SWT) has to be solved for each chemical variable:

$$N_j = \sum_j x_{ij} \cdot \alpha_i \qquad j = 1 \text{ to } n \text{ samples} \qquad (11)$$

Where α_i (≥ 0) is the linear fitting parameter of SWT i. The determination coefficient (R^2) and the standard deviation of the residuals (SD res) of this non–negative least squares analysis are summarized in Table 3.

Mixing–biogeochemical model of dissolved organic matter — Given that the relationship between any pair of non–conservative chemical parameters (N_1, N_2) depends upon the mixing of SWTs, the basin scale mineralization from the formation area to the center of mass of each SWT in the study line and the local–scale mineralization around the respective centers of mass, the following linear equation allows modeling the relationship between N_1 and N_2:

$$N_{1j} - \sum_j x_{ij} \cdot \alpha_{1i} = \beta \cdot \left(N_{2j} - \sum_j x_{ij} \cdot \alpha_{2i} \right) \qquad \text{or}$$

$$N_{1j} = \sum_j x_{ij} \cdot \left(\alpha_{1i} - \beta \cdot \alpha_{2i}\right) + \beta \cdot N_{2j} \qquad j = 1 \text{ to } n \text{ samples} \qquad (12)$$

Where N_{1j} and N_{2j} are the concentrations of N_1 and N_2 in sample j; α_{1i} and α_{2i} are the linear fitting parameter of N_1 and N_2 for SWT i, respectively; and β is the fitting parameter of the relationship between N_1 and N_2 independent of the mixing, assuming that such a relationship is linear and homogeneous (i.e., β does not vary) in all the study area. Again, a system of *n* linear mixing equations (one per sample) was solved with eleven unknowns in this case: ten $\alpha_{1i} - \beta \cdot \alpha_{2i}$ parameters (one per SWT) and β. As for the case of Eq. 11, the goodness of this linear mixing–biogeochemical model was tested using the determination coefficient (R^2) and

the standard deviation of the residuals of the least–squares analysis (SD res). These numbers are also summarized in Table 3. In this work we have studied the mixing–biogeochemical relationships between DOC and AOU, DOC and DON, FDOM and AOU, and FDOM and DOC.

Results

Distributions of water masses in the northeast North Atlantic— Six of the ten SWTs were present in more than 5% of the sampled water in the OVIDE 2002 section (*see* $<\%VOL_i>$ in Table 2). They were ordered according to their archetypal pressure: $ENACW_{12}$, SPMW, MW, LSW, ISOW, and LDW. These six SWTs represented 92% of the total volume of water sampled. The remaining four SWTs ($ENACW_{15}$, SAIW, AIW, and DSOW) contribute marginally to the OVIDE 2002 line. Fig. 2 shows the realms of the subtropical thermocline waters ($ENACW_{15}$ + $ENACW_{12}$, $\theta > 12.30$ºC), subpolar thermocline waters ($ENACW_{12}$ + SPMW + SAIW, $\theta < 12.30$ºC), Mediterranean water (MW), Labrador Sea water (LSW), dense overflow waters (DSOW + ISOW), and lower deep water (LDW). We define the realm of SWT i as the region where x_{ij} is > 50%. Briefly, LSW was the dominant SWT, which represented 36.0% of the total volume of water sampled and extended all along the OVIDE 2002 line at an archetypal depth of 1516×10^{-4} Pa (Table 2), although it was the dominant water mass from the surface to about 2000×10^{-4} Pa north of 59ºN (Fig. 2). The subpolar thermocline waters represented all together 27.1% of the total volume of the water sampled, and they were the dominant water masses in the upper 1000×10^{-4} Pa south of 51ºN. An isolated core of subpolar thermocline waters was observed around 58º 30'N, 30ºW, in between the two branches of LSW that entered the Irminger and Iceland basins, to the west and east of the Reykjanes ridge, respectively. This core was extensively described in Thierry

et al. (2008). A small volume of Mediterranean water was observed in the southern end of the section (Fig. 2), where it was the dominant water mass in the Iberian basin at a narrow depth interval centered around 1255×10^{-4} Pa (Table 2). The dense overflows waters, which represented 11% of the total volume of collected water, dominated the bottom layer of the Irminger and Iceland basins (Fig. 1). Whereas the ISOW meandered anticyclonically around the Reykjanes ridge, the DSOW concentrated on the eastern Greenland slope in the Irminger basin. Finally, the LDW, which is the diluted Antarctic bottom water (AABW) that enters the eastern North Atlantic across the Vema fracture at about 11ºN (McCartney et al. 1991), was the dominant water mass from 3000×10^{-4} Pa to the bottom, south of 53ºN (Fig. 2). It represented 13% of the total volume of water sampled. A detailed description of the water masses distribution and circulation of the northeast North Atlantic, which is out of the scope of this paper, can be found in Álvarez et al. (2004) and Lherminier et al. (2007).

Distributions of chemical parameters in the northeast North Atlantic— The distributions of NO_3, DON, and FDOM along the OVIDE 2002 section are presented in Fig. 3. Trends in the water mass distributions described in Fig. 2 can also be observed in the variability of these chemical tracers. For the case of NO_3 (Fig. 3a), the subtropical thermocline waters south of 49ºN or the dense overflows waters around the Reykjanes ridge were characterized by NO_3 concentrations lower than the surrounding waters. The isolated volume of subpolar thermocline waters around 58º 30'N, 30ºW was also characterized by a relative NO_3 minimum. The isoline of 17 μmol kg^{-1} of NO_3 was a suitable tracer for the dispersion of LSW along the OVIDE 2002 and the LDW was characterized by NO_3 concentrations above 20 μmol kg^{-1}. For the case of DON (Fig. 3b), relatively low (<3 μmol kg^{-1}) concentrations were clearly associated to the MW and LDW realms, and DON minima

were also observed in the area of the dense overflows waters. On the contrary, LSW and specially the thermocline waters, were characterized by relatively high DON levels. Finally, for the case of FDOM (Fig. 3c), there were marked similarities with NO_3 and DON such as the minimum FDOM in the subtropical thermocline waters coinciding with minimum NO_3 and maximum DON levels; the isolated maximum of subpolar thermocline waters around 58º 30'N, 30ºW that coincided again with a NO_3 minimum and DON maximum; or the absolute maximum concentrations in the LDW realm that coincided with the absolute NO_3 maximum and DON minima.

DOM characterization of the water masses of the northeast North Atlantic— The vertical profile of archetypal concentrations of DOC (Fig. 4a) shows that the shallowest thermocline waters of the northeast North Atlantic, between 12ºC ($ENACW_{12}$; centered at 44ºN, 280×10^{-4} Pa) and 15ºC ($ENACW_{15}$; centered at 42ºN, 128×10^{-4} Pa), were characterized by maximum concentrations ranging from 54.8 ± 0.6 to 57.1 ± 1.2 to μmol kg^{-1}. These concentrations were significantly higher ($p < 0.05$), from 1.4–3.7 to 10.7–13.0 μmol kg^{-1}, than the archetypal DOC of the other water masses. On the contrary, the archetypal DOC of the deepest SWT, LDW (centered at 44ºN, 3700×10^{-4} Pa), 44.1 ± 0.5 μmol kg^{-1}, was significantly lower ($p < 0.005$) than the others. At the intermediate waters realm (1000–2000×10^{-4} Pa), it was remarkable that the archetypal DOC of the MW (centered at 41ºN, 1255×10^{-4} Pa), 47.3 ± 0.7 μmol kg^{-1}, was significantly lower ($p < 0.01$) than for LSW (centered at 54ºN, 1516×10^{-4} Pa), 48.9 ± 0.3 μmol kg^{-1}. The profiles of archetypal DOC and AOU (Fig. 4b) were opposite. In fact, the linear relationship with $<AOU_i>$ (Fig. 5a) explained 88% of the variability of $<DOC_i>$:

$$<DOC_i> = 60\ (\pm 1) - 0.20\ (\pm 0.03) \cdot <AOU_i> \qquad R^2 = 0.88,\ n = 10,\ p < 0.001 \qquad (13)$$

Note that, according to our conceptual model, the archetypal AOU retained the variability due to organic matter oxidation from the area of formation of the different SWT to their respective centers of mass (<LON_i>, <LAT_i,>, and <Z_i>**;** Table 2) along the OVIDE line. Therefore, Eq. 13 indicates a tightly coupling between DOC and dissolved oxygen consumption at the northeast Atlantic basin–scale.

For the case of DON, we obtained a constant archetypal concentration of 2.9–3.0 μmol kg^{-1} for the water mass realms below 1000×10^{-4} Pa , except for the case of LSW, which exhibited a significantly higher ($p < 0.01$) archetypal concentration of 3.4 ± 0.2 μmol kg^{-1} (Fig. 4c) . As for DOC, the highest concentrations were obtained in the shallowest thermocline waters, ranging from 4.2 ± 0.1 to 4.7 ± 0.2 μmol kg^{-1}. The profile of archetypal DON explained 94% of the variability of the profile of archetypal DOC (Fig. 5b):

$$<DOC_i> = 26\ (\pm 2) + 6.9\ (\pm 0.6) \cdot <DON_i> \qquad R^2 = 0.94,\ n = 9,\ p < 0.001 \qquad (14)$$

Again, Eq. 14 indicates a tightly coupling between DOC and DON at the northeast Atlantic basin–scale. An exception to this rule was the DSOW realm, with an unexpectedly high archetypal DOC although this value was uncertain (*see* the large standard deviation of the estimate) because the DSOW represented only 1% of the sampled volume of water (Table 2).

The archetypal C:N ratio of DOM (<DOC_i>:<DON_i>; Fig. 4d), increased monotonically with depth, from a minimum of 12.1 ± 0.1 for the shallowest ($ENACW_{15}$) to a maximum of 15.4 ± 0.1 mol C mol N^{-1} for the deepest SWT (LDW; Fig. 5c). <DOC_i>:<DON_i> in the northeast North Atlantic can be reasonably modeled with the following power function of the archetypal pressure:

$$\frac{<\mathrm{DOC_i}>}{<\mathrm{DON_i}>} = 10.3(\pm 0.4) \cdot \left(<\mathrm{Z_i}> - 100\right)^{0.050 \pm 0.006} \qquad R^2 = 0.91,\ n = 8,\ p < 0.001 \qquad (15)$$

This means that the C:N molar ratio of DOM at the base of the photic layer (100×10^{-4} Pa) would be 10.3 ± 0.4 and that it would increase with pressure with a power fitting parameter of 0.050 ± 0.006, independently of the water mass. An exception to this rule was the MW realm, with an archetypal C:N molar ratio of 15.9 ± 0.1, which was significantly higher ($p < 0.001$) than the other intermediate water mass, the LSW, characterised by an archetypal C:N molar ratio of 14.5 ± 0.3. A second exception was the DSOW, with a high archetypical C:N molar ratio of 17.1 ± 1.5.

The behavior of MW compared with LSW can be straightforwardly explained on basis of their contrasting archetypal AOU: 47 ± 2 μmol kg^{-1} for LSW vs. 76 ± 2 μmol kg^{-1} for MW (Fig. 4b). This means that MW aged more than LSW from their respective formation areas to their respective centers of mass in the OVIDE line. In fact, the linear relationship with $\mathrm{AOU_i}$ (Fig. 5d) explained 85% of the variability of $<\mathrm{DOC_i}>:<\mathrm{DON_i}>$:

$$<\mathrm{DOC_i}>:<\mathrm{DON_i}> = 11.5\ (\pm 0.4) + 0.06\ (\pm 0.01) \cdot <\mathrm{AOU_i}> \qquad R^2 = 0.85,\ n = 9,\ p < 0.001 \qquad (16)$$

In this case, DSOW was excluded from the analysis. Therefore, the DOM exported to the northeast Atlantic through the Demark strait was exceptionally carbon–rich in origin.

The profile of archetypal concentrations of FDOM (Fig. 4e) also resembled $<\mathrm{DOC_i}>$ (Fig. 4a) and $<\mathrm{AOU_i}>$ (Fig. 4b) with a minimum value of 0.65 ± 0.04 QSU for the shallowest and a maximum value of 1.23 ± 0.2 QSU for the deepest one. The linear relationships with $<\mathrm{DOC_i}>$ (Fig. 5e) and $<\mathrm{AOU_i}>$ (Fig. 5f) explained 99% and 83% of the variability of $<\mathrm{FDOM_i}>$, respectively:

$$<FDOM_i> = 3.2\ (\pm 0.1) - 0.044\ (\pm 0.002) \cdot <DOC_i> \qquad R^2 = 0.99,\ n = 9,\ p < 0.001 \qquad (17)$$

$$<FDOM_i> = 0.54\ (\pm 0.07) + 0.009\ (\pm 0.002) \cdot <AOU_i> \qquad R^2 = 0.83,\ n = 9,\ p < 0.001 \qquad (18)$$

DSOW was excluded from the analysis because its archetypal FDOM was remarkably high. Therefore, the DOM exported to the northeast Atlantic through the Demark strait was not only carbon–rich but also humic–rich in origin.

Finally, the archetypal C–specific FDOM ratio (Fig. 4f) was also very well correlated with $<AOU_i>$, excluding again the DSOW realm ($<FDOM_i>:<DOC_i> = 0.007\ (\pm 0.002) + 2.5\ (\pm 0.4) \times 10^{-4} \cdot <AOU_i>$, $R^2 = 0.86$, $n = 9$, $p < 0.001$). The fitting parameters of this equation, as well as of Eqs. 13 to 18, were calculated applying regression model II (Sokal and Rolf, 1995) as revised by Castro et al. (2006).

SWT mixing vs. biogeochemistry as drives of the distribution of chemical parameters in the northeast North Atlantic— The mixing of water masses plus the basin scale mineralization retained by the archetypal concentrations explained 62%, 57%, and 76% of the total variability of DOC, DON, and FDOM along the OVIDE 2002 line, respectively (Table 3). The standard error of the residuals (SD res) of the mixing model (Eq. 11), was ±3.1 μmol kg^{-1} for DOC, ±0.5 μmol kg^{-1} for DON and ±0.10 QSU for FDOM, i.e., 4.4 times the measurement error of DOC, 1.5 times the measurement error of DON and 2.7 times the measurement error of FDOM. Therefore, although mixing plus mineralization from the formation area of the water masses to the study OVIDE 2002 line is responsible for more than a half of the variability observed in the global distribution of these variables, in the case of DOC and FDOM the values of SD res were too high to reasonably model their distributions. The non–negative least squares analysis of Eq. 11 was also applied to AOU considering only the 333 samples where DOC, DON and FDOM were measured. The mixing of water masses

plus the basin scale mineralization explained 87% of the total variability of AOU and the SD res, ±10.6 μmol kg^{-1}, was an order of magnitude above the analytical error of the determination of this variable.

Table 3 also show the results of the mixing–biogeochemical model fitted with Eq. 12 for the (N_1, N_2) pairs: (DOC, AOU), (DOC, DON), (FDOM, AOU), and (FDOM, DOC). Although the β value of the (DOC, AOU) pair was highly significant ($p < 0.001$), the SD res of the mixing–biogeochemical model did not improve substantially compared with the mixing model (it reduced only by 3%). Therefore, the β value was just a model artefact and was not reported (Table 3). On the contrary, a substantial reduction of SD res (by > 10%) was obtained for the (DOC, DON) and (FDOM, AOU) pairs. In these two cases, the corresponding β values indicate that the average C:N molar ratio of DOM mineralization around the mass centers of the water masses present in the OVIDE 2002 line, i.e., the DOM mineralised locally, was 13 ± 2 mol C mol N^{-1} and that the production of FDOM was linked to the respiration of organic materials with an average conversion factor of $-8.6 \pm 0.6 \times 10^{-3}$ g equivalent of QS mol O_2^{-1} (Table 3).

This mixing–biogeochemical model can also be applied individually to the six water mass realms previously defined in Fig. 2. For the case of the subtropical thermocline waters, only the (DOC, DON) and (FDOM, AOU) models experienced a substantial reduction, by 8% and 58% respectively, of the SD res compared with the corresponding mixing models. The β values suggest that the C:N molar ratio of mineralization around the mass center of the SWT that contribute to this realm ($ENACW_8$ and $ENACW_{15}$) was 13 ± 5 mol C mol N^{-1} and that the conversion factor of O_2 consumption to FDOM production was $-15 \pm 1 \times 10^{-3}$ g equivalent of QS mol O_2^{-1} (Table 3). In the subpolar thermocline waters, the (DOC, AOU), (DOC, DON) and (FDOM, AOU) models experienced substantial SD res reductions of 5%, 15%, and

33% compared with the corresponding mixing models. The β values were –0.27 ± 0.08 mol C mol O_2^{-1}, 11 ± 2 mol C mol N^{-1} and –7.0 ± 0.7 $\times 10^{-3}$ g equivalent of QS mol O_2^{-1}. For the case of the Mediterranean water realm, only the (DOC, DON) model experienced a substantial reduction (by 40%) of the SD res, and the corresponding β values was 13 ± 3 mol C mol N^{-1}. In the Labrador Sea water realm, the (DOC, AOU) and (FDOM, AOU) models showed SD res reductions >10%, with β values of –0.45 ± 0.09 mol C mol O_2^{-1} and –9 ± 2 $\times 10^{-3}$ g equivalent of QS mol O_2^{-1}. In the dense overflows of the northern North Atlantic, the mixing–biogeochemical model did not improved significantly the predictions of the mixing model alone, likely because only 11 of the 333 samples belong to this realms, a reduced number of data points for our statistical approach. Finally, in the lower deep water realm only the (DOC, DON) model experienced a substantial reduction of the SD res, and the obtained β was 11 ± 5 mol C mol N^{-1}. Therefore, depending on the pairs of variables, specific values of β can be obtained for the different water mass realms.

Discussion

The statistical method applied in this work allowed to objectively separate: The effect of water mass mixing and basin–scale mineralization from the formation area to the center of mass of the ten SWT intercepted along the OVIDE 2002 line (retained by the mixing model); from the effect of local mineralization around the center of mass of each SWT (retained by the fitting parameter β of the mixing–biogeochemical model).

Contribution of dissolved vs. particulate organic matter to the oxygen demand of the northeast North Atlantic— Our profile of archetypal concentrations of DOC can be compared with the values reported by Carlson et al. (2010) for the whole North Atlantic. Our upper and lower thermocline values of 54.8–57.1 and 50.5–54.8 μmol kg^{-1}, respectively, were quite

comparable to those reported by Carlson et al. (2010). Regarding the LSW and ISOW, our archetypal concentrations where 5–6 μmol kg^{-1} higher, probably because the OVIDE 2002 line was much closer to the formation area of these water masses than the Climate Variability (CLIVAR) lines studied by Carlson et al. (2010). The difference was even larger, 9 μmol kg^{-1}, for the case of the DSOW. The high DOC concentration, C:N ratio of DOM and humic–like fluorescence of this water mass will receive particular attention in the following sections. Finally, regarding the LDW, our archetypal concentration, 44.1 ± 0.5 μmol kg^{-1}, was 3.6 μmol kg^{-1} above the DOC of Antarctic bottom water (AABW) reported by Carlson et al. (2010), but note that whereas the archetypal depth of our LDW was 3700 ± 159 10^{-4} Pa , the average depth of AABW was 5019 10^{-4} Pa . Regarding the archetypal DOC concentration of MW, 47.3 ± 0.7 μmol kg^{-1}, it was significantly lower than the expected concentration of 48.8–49.3 μmol kg^{-1} obtained when mixing the Mediterranean overflow water (MOW) of the Strait of Gibraltar (45–46 μmol kg^{-1}; Dafner et al. 2001) with the SPMW (50.5 ± 0.6 μmol kg^{-1}; Fig. 4a) in a MOW:SPMW proportion of 0.25–0.34 to form the MW (Rogerson et al. 2012). These numbers indicate that intense mineralisation of DOM occurs during the subduction of MOW and the entrainment of SPMW to form MW.

The excellent linear relationship between the archetypal concentrations of DOC and AOU (Fig. 5a) suggest that the basin–scale mineralization of dissolved organic matter from the formation area of the SWT to their respective centers of mass along the OVIDE 20202 line in the northeast North Atlantic can be modeled assuming a quasi–constant concentration of DOC of 60 ± 1 μmol kg^{-1} (y–intercept of Eq. 13) at the time of formation of the different SWT (AOU = 0.0 μmol kg^{-1}), which decreased with increasing AOU at a rate of 0.20 ± 0.3 mol C mol O_2^{-1}. Considering the Redfieldian R_N and R_P values of 9.4 ± 0.3 mol O_2 mol N^{-1} and 162 ± 5 mol O_2 mol P^{-1} retained by the OMP analysis, a $-O_2$: Corg stoichiometric ratio

(R_C) of 1.4 mol O_2 mol C^{-1} (Redfield et al. 1963; Anderson and Sarmiento 1994) can be used to estimate a basin–scale contribution of DOC to the oxygen demand of the northeast North Atlantic of 28 ± 4% from the slope of 0.20 ± 0.3 mol C mol O_2^{-1} (Eq. 13). Considering the water mass realms defined in Fig. 2 individually, AOU improved the prediction of the distribution of DOC only for the subpolar thermocline waters and Labrador Sea water realms. In the case of the subpolar thermocline waters, the value of β suggests that 40 ± 10% of the local oxygen demand around the center of mass of this water mass was covered by DOC and in the case of the Labrador Sea water realm, the contribution of DOC increased to as much as 60 ± 10%. Our estimate of the basin–scale contribution of DOC to the oxygen demand of the northeast North Atlantic is in the upper end of the calculations of Arístegui et al. (2002) for the global mesopelagic ocean and those of Carlson et al. (2010) for the whole North Atlantic basin. This is an expected result considering that the OVIDE line was very close to the formation areas of the LSW, DSOW, ISOW, and MW and intercepted the formation areas of the ENACW and SPMW. The closer a water mass is to its formation area, the higher is the contribution of DOC to the oxygen demand on the realm of that water mass because the concentration of DOC is higher and probably more bioavailable. Thus, 30–40% of the microbial respiration at intermediate depths of the North Pacific was due to the oxidation of the DOM transported downwards by the North Pacific intermediate water (Doval and Hansell 2000; Hansell et al. 2012). In the North Atlantic, Carlson et al. (2010) obtained that the export and subsequent mineralization of DOC explained 9–19% of the oxygen demand in the North Atlantic deep water, when it explained <10% in the deep Pacific and Indian Oceans (Doval and Hansell 2000). The case of MW merits attention because DOC does not contribute significantly to the oxygen demand. As indicated above, this SWT is composed of the diluted Levantine intermediate water (LIW) that crosses the sill of the Strait of Gibraltar and

subducted North Atlantic thermocline waters (Álvarez et al. 2005). Considering the relatively high respiration rates measured by La Ferla and Azzaro (2004) in the LIW, from 4 μmol C kg^{-1} yr^{-1} in the Levantine basin to 1 μmol C kg^{-1} yr^{-1} in the Strait of Gibraltar, it is likely that most of the mineralization of the DOM carried by the MW, which results in its high $<DOC_i>$: $<DON_i>$ ratio (Fig. 4d), has occurred within the Mediterranean Sea. In fact, Santinelli et al. (2010) reported that DOC contributed to 38% of the oxygen demand on the LIW realm. In addition, intense mineralisation seems to occur during the entrainment of the Mediterranean overflow water and North Atlantic thermocline waters to form the MW (*see* previous paragraph).

Stoichiometry of the mineralization of dissolved organic matter in the northeast North Atlantic— Although the C:N ratios of DOM (Fig. 4d) were comparable with the average global deep ocean ratio of 14.7 ± 2.8 mol C mol N^{-1} compiled by Bronk (2002), it is remarkable the exceptional linear relationship obtained between the archetypal concentrations of DOC and DON (Fig. 5b). The regression slope of 6.9 ± 0.3 mol C mol N^{-1} indicates that the C:N ratio of the DOM mineralised at the basin–scale from the formation areas of the SWT to their respective center of mass along the OVIDE 2020 line does not differ significantly from the Redfieldian ratio of 6.7, characteristic of the mineralisation of fresh fast–sinking phytogenic particles (Redfield et al. 1963; Anderson and Sarmiento 1994). The preferential use of the N–rich compounds of particulate organic matter is well documented from the increasing C:N ratio of the material collected on sediment traps with depth (Schneider et al. 2003) or the study of inorganic nutrient ratios (Brea et al. 2004; X.A. Álvarez–Salgado unpubl.). Our work provides evidences that the DOM consumed in the dark ocean follows the same pattern, supporting observations made in ocean margins and central ocean gyre environments indicating that DOM is mineralized with a C:N:P stoichiometry substantially

lower than for bulk pools (Hopkinson and Vallino 2005; Álvarez–Salgado et al. 2006). Hopkinson and Vallino (2005) reported that although the C: N: P stoichiometry of DOM mineralization is lower than for the bulk DOM, it is greater than the Redfield ratio. Since their open ocean profiles were collected in central gyres, its seems that the Redfield stoichiometry found in the OVIDE 2002 line could be characteristic of intermediate and deep ocean ventilation sites. This basin–scale DOM consumption with a C:N molar ratio of 6.9 produced a highly significant ($p < 0.001$) increase of the archetypal C:N ratio of DOM with increasing AOU (Fig. 5d), which results in aged water masses being characterized by high C:N ratios of DOM because of preferential consumption of the more labile N–rich DOM compounds (Hopkinson and Vallino 2005; Kramer et al. 2005). Accordingly, the evolution of the C:N ratio of DOM in the northeast North Atlantic result from a quasi–constant ratio of 11.5 ± 0.4 mol C mol N^{-1} (y–intercept of Eq. 16) at the time of formation (AOU = 0.0 μmol kg^{-1}) of the different SWT that mix in the OVIDE line, which increases with increasing AOU at a rate of 0.06 ± 0.01 (mol C mol N^{-1}) per mol of AOU. Only the DSOW was clearly apart from that straight line (Fig. 5d).

Considering the whole data set ($n = 333$), it resulted that the mixing–biogeochemical model improved the prediction of the distribution of DOC when DON is considered as explanatory variable (Table 3), which means that not only the basin–scale but also the local–scale processes in the surrounding of the mass center of each water mass along the OVIDE line are necessary to describe the DOM distributions. Interestingly, the value of the corresponding β parameter indicates that the C:N ratio of local DOM mineralization around the mass center of the water masses that mix along the OVIDE line increased to a significantly higher ($p < 0.001$) value of 13 ± 2 mol C mol N^{-1}. The C:N molar ratios of local mineralization in the subtropical (13 ± 5) and subpolar (11 ± 2) thermocline, Mediterranean

(13 ± 3) and Lower Deep Water (11± 5) realms did not differed significantly. This is consistent with the mineralisation of fresh dissolved and fast–sinking biogenic materials close to the formation area of the water masses (retained by the mixing model), where they suddenly sank from the surface to their respective archetypal depths (Brea et al. 2004; X.A. Álvarez–Salgado unpubl.). By contrast, local mineralisation (retained by the fitting parameter β of the mixing–biogeochemical model) would be supported by slow sinking suspended materials and aged DOM transported downwards from the upper mixed layer.

Production of marine humic–like substances in the northeast North Atlantic— Marine humic–like substances in the dark ocean are a by–product of the microbial respiration of biogenic organic matter, either dissolved or particulate (Yamashita and Tanoue 2008; Jørgensen et al. 2011). Therefore, the positive linear relationship found between archetypal FDOM and AOU (Fig. 5f) was sound and the slope of this correlation can be used as an indicator of the recovery of marine humic–like substances from the degradation of organic matter. A good correlation was also observed between archetypal FDOM and DOC (Fig. 5e), suggesting that both fast–sinking fresh biogenic particles and DOM contribute to the basin–scale production of humic–like materials in the water masses that mix in the northeast North Atlantic. Using a R_C of 1.4 mol O_2 mol C^{-1}, it results that the rate of FDOM production to organic carbon mineralisation ―either dissolved, suspended or sinking― would be –13 ± 3 $\times 10^{-3}$ g equivalent of QS mol C^{-1} (= –9 ± 2 $\times 10^{-3}$ g equivalent of QS mol O_2^{-1} × 1.4 mol O_2 mol C^{-1}). For comparison, the rate of FDOM production to DOC mineralisation was 44 ± 2 $\times 10^{-3}$ g equivalent of QS mol C^{-1}. Multiplying this rate by the contribution of DOC to the basin–scale oxygen demand of the northeast North Atlantic, 28 ± 4%, yields a rate of –12 ± 2 $\times 10^{-3}$ g equivalent of QS mol C^{-1}, which is not significantly different from the value –13 ± 3

$\times 10^{-3}$ g equivalent of QS mol C^{-1}. Therefore, the rate of FDOM formation is not dependent on the aggregation state of the mineralised organic matter. Again, only the DSOW was clearly apart from that straight line. The DOM exported to the northeast Atlantic through the Demark Strait is carbon– and humic–rich in origin, likely due to a larger terrestrial influence. Note that the DSOW (salinity 34.88; Table 3) is 0.3% fresher than the ISOW (salinity 34.98). Following Amon et al. (2003) and Benner et al. (2005), surface waters of the Arctic Ocean have the highest concentrations of DOC and terrigenous DOM (from Arctic rivers) of all ocean basins and these materials are exported to the ocean interior preferentially in the DSOW. Furthermore, lignin phenols of terrestrial origin (Benner et al. 2005) are the likely cause of the enhanced archetypal humic–like fluorescence of the DSOW (Ammon et al. 2003; Osburn and Stedmon 2011).

Regarding the production of humic–like substances during the local degradation of organic matter, the value of β for the whole dataset (n = 333), $-8.6 \pm 0.6 \times 10^{-3}$ g equivalent of QS mol O_2^{-1}, was not significantly different from the value obtained for the basin–scale mineralization (Eq. 18). However, the efficiency of humic–like substances production depended on the water mass realm. The parameter β for the Labrador Sea water was not significantly different from the β for the whole set of samples; an expected result considering that LSW was the most densely sampled water mass, appearing in 33% of the 333 samples collected. However, the β of the subtropical thermocline waters ($-15 \pm 1 \times 10^{-3}$ g equivalent of QS mol O_2^{-1}) was significantly higher ($p < 0.001$) and the β of the subpolar thermocline waters ($-7.0 \pm 0.7 \times 10^{-3}$ g equivalent of QS mol O_2^{-1}) was significantly lower ($p < 0.005$) than the reference value of $-8.6 \pm 0.6 \times 10^{-3}$ g equivalent of QS mol O_2^{-1}. Note that the archetypal AOU of $ENACW_{12}$ (31 ± 3 μmol kg^{-1}), the dominant SWT in the subtropical thermocline waters realm, was significantly lower ($p < 0.001$) than the archetypal AOU of the

LSW (47 ± 2 μmol kg^{-1}) and the latter was significantly lower ($p < 0.001$) than the archetypal AOU of the SPMW (52 ± 4 μmol kg^{-1}), the dominant SWT of the subpolar thermoclime waters realm. Therefore, it seems that the efficiency of the local production of humic–like substances from the consumption of biogenic materials is directly proportional to the ventilation of the corresponding SWT realms. This hypothesis is confirmed by the low conversion factors, –4.7 to –4.9 $\times 10^{-3}$ g equivalent of QS mol O_2^{-1}, that Yamashita and Tanoue (2008) obtained in the very aged thermocline (AOU, 25–300 μmol kg^{-1}) and abyssal (AOU, 150– 300 μmol kg^{-1}) waters of the Pacific Ocean. Conversely, Yamashita et al. (2007) obtained higher conversion factors of –6.4 ± 1.0 and –6.8 ± 0.8 $\times 10^{-3}$ g equivalent of QS mol O_2^{-1} for the more ventilated subantarctic mode water (SAMW) and Antarctic intermediate water (AAIW) in the Pacific sector of the Southern Ocean. Finally, in the Iberian upwelling system, Castro et al. (2006) obtained a conversion efficiency of –7.8 ± 0.4 g equivalent of QS mol O_2^{-1} for the central waters off NW Spain and Nieto–Cid et al (2006) a value of –8.1 ± 0.9 $\times 10^{-3}$ g equivalent of QS mol O_2^{-1} for the same waters once they have upwelled into the rías, the large coastal embayments of the Galician coast. Consequently, the estimate made by Yamashita and Tanoue (2008) of the global production of FDOM in the ocean interior, 13–17 $\times$ 10^{12} g equivalent of QS yr^{-1}, is probably underestimated by one–third.

References

Álvarez, M., F. F. Pérez, H. L. Bryden, and A. F. Ríos. 2004. Physical and biogeochemical transports structure in the North Atlantic subpolar gyre. J. Geophys. Res. **109**: C03027, doi: 10.1029/2003JC002015

Álvarez, M., F. F. Pérez, D. R. Shoosmith, and H. L. Bryden. 2005. The unaccounted role of Mediterranean water in the draw–down of anthropogenic carbon. J. Geophys. Res. **110**: C09S03, doi: 10.1029/2004JC002633

Álvarez–Salgado, X. A., M. Nieto–Cid, J. Gago, S. Brea, C. G. Castro, M. D. Doval, and F. F. Pérez. 2006. Stoichiometry of the mineralization of dissolved and particulate biogenic organic matter in the NW Iberian upwelling. J. Geophys. Res. **111**: C07017, doi: 10.1029/2004JC002473

Ambar, I., and M. R. Howe. 1979. Observations of the Mediterranean outflow– I: Mixing in the Mediterranean outflow. Deep–Sea Res. **26**: 535–554.

Amon, R. M. W., G. Budéus, and B. Meon. 2003. Dissolved organic carbon distribution and origin in the Nordic seas: Exchanges with the Arctic Ocean and the North Atlantic. Journal of Geophysical Research **108**: 3221, doi: 10.1029/2002JC001594

Anderson, L. A., and J. L. Sarmiento. 1994. Redfield ratios of remineralization determined by nutrient data analysis. Global Biogeochem. Cy. **8**: 65–80.

Arhan, M. 1990. The North Atlantic current and subarctic intermediate water. J. Mar. Res. **48**: 109–144.

Arístegui J., C. M. Duarte, S. Agustí, M. D. Doval, X. A. Álvarez–Salgado, and D. A. Hansell. 2002. Dissolved versus particulate organic carbon consumption in the dark ocean. Science **298**: 1967.

Benner, R., P. Lauchouran, and R. M. W. Amon. 2005. Terrigenous dissolved organic matter in the Arctic Ocean and its transport to surface and deep waters of the North Atlantic. Global Biogeochem. Cy. **19**: GB2025, doi: 10.1029/2004GB002398

Brea, S., X. A. Álvarez–Salgado, M. Álvarez, F. F. Pérez, L. Mémery, H. Mercier, and M. J. Messias. 2004. Nutrient mineralization rates and ratios in the eastern South Atlantic. J. Geophys. Res. **109**: C05030, doi: 10.1029/2003JC002051

Bronk, D. A. 2002. Dynamics of DON, p. 153–247. *In* D.A. Hansell, and C.A. Carlson [eds.], Biogeochemistry of marine dissolved organic matter. Academic Press.

Carlson, C. A., D. A. Hansell, N. B. Nelson, D. A. Siegel, W. M. Smethie, S. Khatiwala, M. M. Meyers, and E. Halewood. 2010. Dissolved organic carbon export and subsequent remineralization in the mesopelagic and bathypelagic realms of the North Atlantic basin. Deep-Sea Res. II **57**: 1433–1445.

Castro, C. G., M. Nieto–Cid, X. A. Álvarez–Salgado, and F. F. Pérez. 2006. Local mineralization patterns in the mesopelagic zone of the eastern North Atlantic of the NW Iberian Peninsula. Deep-Sea Res. I **53**: 1925–1940.

Coble, P. G. 1996. Characterization of marine and terrestrial DOM in seawater using excitation–emission matrix spectroscopy. Mar. Chem. **51**: 325–346.

Dafner, E. V., R. Sempere, and H. L. Bryden. 2001. Total organic carbon distribution and budget through the Strait of Gibraltar in April 1998. Mar. Chem. **73**: 233–252.

Dickson, R., and J. Brown. 1994. The production of North Atlantic deep water: Sources, rate and pathways. J. Geophys. Res. **99**: 12319–12341.

Doval, M. D., and D. A. Hansell. 2000. Organic carbon and apparent oxygen utilization in the western South Pacific and the central Indian Oceans. Mar. Chem. **68**: 249–264.

Hansell, D. A., and C. A. Carlson. 1998. Deep–ocean gradients in the concentration of dissolved organic carbon. Nature **395**: 263–266.

Hansell, D. A., C. A. Carlson, and Y. Suzuki. 2002. Dissolved organic carbon export with North Pacific intermediate water formation. Global Biogeochem. Cy. **16**: 1007, doi: 10–1029/2000GB001361

Hansell, D. A., C. A.Carlson, D. J. Repeta, and R. Schlitzer. 2009. Dissolved organic matter in the ocean: New insights stimulated by a controversy. Oceanography **22**: 52–61

Hansell, D. A., C. A.Carlson, and R. Schlitzer. 2012. Net removal of major marine dissolved organic carbon fractions in the subsurface ocean. Global Biogeochem. Cy. **26**: GB1016, doi: 10.1029/2011GB004069

Harvey, J. 1982. θ–S relationship and water masses in the eastern North Atlantic. Deep–Sea Res. **29:** 1021–1033.

Harvey, J. G., and M. Arhan. 1988. The water masses of the central North Atlantic in 1983–84. J. Phys. Oceanogr. **18**: 1855–1875.

Harvey, J. G., and A. Theodorou. 1986. The circulation of Norwegian Sea overflow water in the eastern North Atlantic. Oceanol. Acta **9**: 393–402.

Hopkinson Jr., C. S., and J. J. Vallino. 2005. Efficient export of carbon to the deep ocean through dissolved organic matter. Nature **433**: 142–145.

Jahnke, R. 1996. The global ocean flux of particulate organic carbon: Areal distribution and magnitude. Global Biogeochem. Cy. **10**: 71–88.

Jørgensen, L., C. A. Stedmon , T. Kragh, S. Markager, M. Middelboe, and M. Søndergaard. 2011. Global trends in the fluorescence characteristics and distribution of marine dissolved organic matter. Mar. Chem. **126**: 139–148.

Kramer, G. D., C. Pausz, C., and G. J. Herndl. 2005. Elemental composition of dissolved organic matter and bacterioplankton production in the Faroe – Shetland Chanel (North Atlantic). Deep-Sea Res. I **52**: 85–97.

La Ferla, R., and M. Azzaro. 2004. Metabolic CO_2 production in the Mediterranean Sea: A case study for estimating carbon budget in the sea. Sci. Mar. **68**: 57–64.

Lee, A., and D. J. Ellett. 1967. On the water masses of the northwest Atlantic Ocean. Deep–Sea Res. **14**: 183–190.

Lherminier, P., H. Mercier, C. Gourcuff, M. Álvarez, S. Bacon, and C. Kermabon. 2007. Transports across the 2002 Greenland–Portugal Ovide section and comparison with 1997. J. Geophys. Res. **112**: C07003, doi: 10.1029/2006JC004716

McCartney, M. S. 1992. Recirculating components of the deep boundary current of the northern North Atlantic. Progr. Oceanogr. **29**: 283–383.

McCartney, M. S., S. L. Bennett, M. E. Woodgate–Jones. 1991. Eastward flow through the Mid–Atlantic Ridge at 11ºN and its influence on the abyss of the eastern basin. J. Phys. Oceanogr. **14**: 922–935.

McCartney, M. S. 1982. The subtropical recirculation of mode waters, J. Mar. Res. **40**: 427-464.

McCartney, M. S., and L. D. Talley. 1982. The subpolar mode water of the North Atlantic Ocean. J. Phys. Oceanogr. **12**: 1169–1188.

Nieto–Cid, M., X. A. Álvarez–Salgado, and F. F. Pérez. 2006. Microbial and photochemical reactivity of fluorescent dissolved organic matter in a costal upwelling system. Limnol. Oceanogr. **51**: 1391–1400.

Osburn C. L., and C. A. Stedmon. 2011. Linking the chemical and optical properties of dissolved organic matter in the Baltic–North Sea transition zone to differentiate three allochthonous inputs. Mar. Chem. **126**: 281–294.

Pérez, F. F., C. Mouriño, F. F. Fraga, and A. F. Ríos. 1993. Displacement of water masses and remineralization rates off the Iberian Peninsula by nutrient anomalies. J. Mar. Res. **51**: 1–24.

Pickart, R. S., F. Straneo, G. W. K. Moore. 2003. Is Labrador Sea water formed in the Irminger basin? Deep–Sea Res. I **50**: 23–52.

Pollard, R. T., M. J. Griffiths, S. Cunningham, J. F. Read, F. F. Pérez, and A. F. Ríos. 1996. Vivaldi 1991– A study of the formation, circulation and ventilation of eastern North Atlantic central water. Prog. Oceanogr. **37**:167–192.

Pollard, R. T., and S. Pu. 1985. Structure and circulation of the upper Atlantic Ocean northeast of the Azores. Prog. Oceanogr. **14**: 443–462.

Redfield, A. C., B. H. Ketchum, and F. A. Richards. 1963. The influence of organisms on the composition of seawater, p. 26–77. *In* M. N. Hill [ed.], The sea, Vol. 2. Wiley–Interscience.

Ríos, A. F., F. F. Pérez, and F. Fraga. 1992. Water masses in the upper and middle North Atlantic Ocean east of the Azores. Deep–Sea Res. I **39**: 645–658.

Rogerson, M., E. J. Rohling, G. R. Bigg, and J. Ramirez. 2012. Paleoceanography of the Atlantic-Mediterranean exchange: overview and first quantitative assessment of climatic forcing. Rev. Geophys. **50**: RG2003, doi: 10.1029/2011RG000376

Santinelli, C., L. Nannicini, and A. Seritti. 2010. DOC dynamics in the meso and bathypelagic layers of the Mediterranean Sea. Deep-Sea Res. II **57**:1446–1459

Sarmiento, J. L., and N. Gruber. 2006. Ocean biogeochemical dynamics. Princeton University Press.

Schneider, B., R. Schlitzer, G. Fischer, and E.–M. Nöthing. 2003. Depth–dependent elemental compositions of particulate organic matter (POM) in the Ocean. Global Biogeochem. Cy. **17**: 1032, doi: 10.1029/2002GB001871

Suga, T., and L. D. Talley. 1995. Antarctic intermediate water circulation in the tropical and subtropical South Atlantic, J. Geophys. Res. **100**: 13441-13453.

Swift, J.H. 1984. The circulation of Denmark Strait and Iceland–Scotland overflow waters in the North Atlantic. Deep–Sea Res **31**: 1339–1355.

Talley, L.D., and M.S. McCartney. 1982. Distribution and circulation of Labrador Sea water. J. Phys. Oceanogr. **12**: 1189–1205, 1982.

Thierry, V., E. de Boisséson, and H. Mercier. 2008. Interannual variability of the subpolar mode water property over the Reykjanes Ridge during 1990-2006. J. Geophys. Res. Oceans **113**: C04016, doi:10.1029/2007JC004443

Tsuchiya, M. 1989. Circulation of the Antarctic intermediate water in the North Atlantic Ocean, J. Mar. Res. **47**: 747-755.

Tsuchiya, M., L. D. Talley, and M. S. McCartney. 1992. An eastern Atlantic section from Iceland southward across the equator. Deep–Sea Res **39**: 1885–1917.

van Aken, H. M., and C. J. de Boer. 1995. On the synoptic hydrography of intermediate and deep water masses in the Iceland Basin. Deep–Sea Res. I **42**: 165–189.

Yamashita Y., A. Tsukasaki, T. Nishida, and E. Tanoue. 2007. Vertical and horizontal distribution of fluorescent dissolved organic matter in the Southern Ocean. Mar. Chem. **106**: 498–509.

Yamashita, Y., and E. Tanoue. 2008. Production of bio-refractory fluorescent dissolved organic matter in the ocean interior. Nature Geosciences **1:** 579–582.

Zenk, W. 1975. On the Mediterranean outflow west of Gibraltar. Meteor Forschungs–Ergebnisse A 16, 23–24.

Table 1. Main water masses crossed by the OVIDE 2002 section in the northeast North Atlantic, brief description of their characteristics and some references where more information about their origin and circulation can be found.

Name and acronym	Source	Characteristics	References
Subtropical eastern North Atlantic central water ($ENACW_{15}$)	Subtropical gyre	Mode water formed in the area of the Azores Current, $\theta > 13°C$ and $S > 35.7$, very low nutrient concentration	Pollard and Pu 1985; Ríos et al. 1992
ENACW of 12ºC ($ENACW_{12}$)	Subtropical and Subpolar gyre	Mode water defining the lower limit of subtropical ENACW and the upper limit of SPMW	Harvey 1982; Pollard and Pu 1985
Subpolar mode water (SPMW)	Subpolar gyre	Mode water formed north of 42ºN and east of 20ºW, $\theta < 12°C$ and $S < 35.5$, higher concentration of nutrients than subtropical ENACW	Harvey 1982; McCartney and Talley 1982; Pollard et al. 1996
Antarctic intermediate water diluted (AIW)	Subantarctic front	Intermediate water formed by subduction, identified as a salinity minimum in the South Atlantic, it reaches the North Atlantic with typical silicate maximum signature	McCartney 1982; Tsuchiya 1989; Suga and Talley 1995
Subarctic intermediate water (SAIW)	Subpolar gyre	Not a mode water, originates in the western boundary of subpolar gyre by mixing, $4 < \theta < 7$ºC and $S < 34.9$	Arhan 1990
Mediterranean water (MW)	Gulf of Cadiz	Formed by entrainment of central waters on the high salinity outflow from the Mediterranean Sea, spreads at 800–1300 × 10^{-4} Pa , $S > 36$ and θ ~11°–12°C	Zenk 1975; Ambar and Howe 1979
Labrador Sea water (LSW)	Labrador Sea and Irminger Sea	Formed by winter convection, spreads between 1500–2000 × 10^{-4} Pa , θ ~ 3°C, S ~ 34.8 and, high oxygen content	Talley and McCartney 1982; Harvey and Arhan 1988; Pickart et al. 2003
Iceland Scotland overflow water (ISOW)	Norwegian Sea and sills of Faroe Bank Channel	Formed in the sills by entrainment on the Norwegian overflow, it spreads in the Northern North Atlantic at 2750 ×10^{-4} Pa , $\theta > 2°C$ and $S > 34.94$, high oxygen and low nutrient signature	Swift 1984; Harvey and Theodorou 1986
Denmark Strait overflow water (DSOW)	Arctic Ocean and Denmark Strait	Same formation mechanism as ISOW, well ventilated water, very low temperature, $\theta < 2$ºC, and S from 34.8 to 34.9, high oxygen and low nutrient content	Tsuchiya et al. 1992; van Aken and de Boer 1995
Lower deep water (LDW)	Antarctic Ocean	Warmed Antarctic Bottom water entering at the Vema fracture. In the Iberian basin, θ and S have a linear relation, very high silicate signature	Lee and Ellet 1967; McCartney et al. 1991; McCartney 1992; Dickson and Brown 1994

Table 2. Thermohaline and chemical characteristics of the source water types (SWTs) introduced in the optimum multiparamter (OMP) analysis of the water masses that mix in the northeast North Atlantic. $<LON_i>$, $<LAT_i>$ and $<Z_i>$ are the archetypal longitude, latitude and pressure of SWT i, calculated with Eq. 8. $<\%VOL_i>$ is the contribution of SWT i to the total volume of water collected along the OVIDE 2002 line calculated with Eq. 10. Weight (W), determination coefficient (R^2) and standard deviation of the residuals (SD res) of each parameter explained by the mixing model. Number of samples (n = 1937).

	Z_i ($\times 10^{-4}$ Pa)	$<LON_i>$ (ºW)	$<LAT_i>$ (ºN)	$<\%VOL_i>$	θ_t (ºC)	S_i	SiO_{4i} (μmol kg^{-1})	$O_{2i}{}^0$ (μmol kg^{-1})	$NO_{3i}{}^0$ (μmol kg^{-1})	$PO_{4i}{}^0$ (μmol kg^{-1})
$ENACW_{15}$	128	14.7	42.0	1.8	14.80	36.02	0.9	247	0.2	0.03
SAIW	236	27.0	55.9	4.7	8.00	34.67	6.7	276	8.9	0.72
$ENACW_{12}$	280	17.0	43.8	12.6	12.30	35.66	3.2	260	7.1	0.46
AIW	409	22.3	49.9	0.4	7.40	34.90	11.1	297	14.4	1.05
SPMW	658	23.8	51.8	14.4	8.23	35.24	10.6	286	8.7	0.67
MW	1255	13.9	41.4	5.9	11.74	36.50	9.5	262	5.7	0.38
LSW	1516	25.8	54.4	36.0	2.90	34.85	10.4	323	12.9	0.92
ISOW	2670	25.8	54.4	10.3	2.40	34.98	11.9	328	10.4	0.75
DSOW	2675	39.0	59.6	0.9	0.50	34.88	6.4	344	9.1	0.65
LDW	3700	17.0	43.8	12.8	1.98	34.89	52.4	331	12.6	1.03
W					10	5	3	2	4	0.5
R^2					0.9996	0.9988	0.9996	0.9934	0.9948	0.9854
SD res					±0.07	±0.01	±0.2	±2	±0.3	±0.03

$ENACW_{15}$, subtropical eastern North Atlantic central water of 15ºC; SAIW, Subarctic intermediate water; $ENACW_{12}$, ENACW of 12ºC; AIW, diluted Antarctic intermediate water; SPMW, Subpolar mode water; MW, Mediterranean water; LSW, Labrador Sea water; ISOW, Iceland Strait overflow water; DSOW, Denmark Strait overflow water; and LDW, Lower deep water.

Table 3. Parameters of the linear mixing (Eq. 11) and mixing–biogeochemical (Eq. 12) models. R^2, determination coefficient; SD res, standard deviation of the residuals of the estimation; % SD reduction, percentage of reduction of the SD res of the mixing–biogeochemical as compared with the corresponding mixing model; β, fitting parameter of the relationship between N_1 and N_2 independent of the mixing; SD(β), standard error of the estimation of β; p, significance level of the estimation of β. Results are presented for all samples and for the six water mass realms defined in Fig. 2. Only 29 of 333 samples did not belong to any realm, because they do not have > 50% proportion of any of the 6 SWTs or groups of SWTs defined in Fig. 2. Numbers in parentheses are the contribution of each SWT in each of the study water mass realms.

N_1	N_2	R^2	SD res	% SD reduction	β	SD(β)	p
All water samples (n = 333) SWTs involved: LSW (33%), $ENACW_{12}$ (18%), SPMW (15%), LDW (10%), ISOW (8%) SAIW (6%), MW (5%), $ENACW_{15}$ (3%), DSOW (1%), and AIW (1%)							
DOC		0.62	3.1				
DON		0.57	0.5				
FDOM		0.76	0.10				
AOU		0.87	10.6				
DOC	AOU	0.64	3.00	3%	—	—	0.0000
DOC	DON	0.68	2.80	10%	13	2	0.0000
FDOM	AOU	0.84	0.08	18%	0.0086	0.0006	0.0000
FDOM	DOC	0.76	0.10	0%	—	—	0.0031
Subtropical thermocline waters realm ($ENACW_{15}$ + $ENACW_{12}$ > 50%; n = 38) SWTs involved: $ENACW_{12}$ (69%), $ENACW_{15}$ (30%), and MW (1%)							
DOC		—	4.0				
DON		0.11	0.56				
FDOM		0.07	0.15				
AOU		0.08	10.1				
DOC	AOU	0.01	3.9	1%	—	—	0.2429
DOC	DON	0.15	3.6	8%	13	5	0.0102
FDOM	AOU	0.84	0.06	58%	0.0146	0.0011	0.0000
FDOM	DOC	0.05	0.15	0%	—	—	0.6447

N_1	N_2	R^2	SD res	% SD reduction	β	SD(β)	p
Subpolar thermocline waters realm ($ENACW_{12}$+ SAIW + SPMW > 50%; n = 98) SWTs involved: SPMW (34%), $ENACW_{12}$ (34%), SAIW (16%), LSW (10%), MW (4%), and AIW (2%)							
DOC		0.27	3.5				
DON		0.26	0.49				
FDOM		0.54	0.10				
AOU		0.79	13.0				
DOC	AOU	0.35	3.3	5%	–0.27	0.08	0.0012
DOC	DON	0.47	3.0	15%	11	2	0.0000
FDOM	AOU	0.79	0.07	33%	0.0070	0.0007	0.0000
FDOM	DOC	0.56	0.10	2%	—	—	0.0327
Mediterranean water realm (MW > 50%; n = 14) SWTs involved: MW (62%), SPMW (28%), $ENACW_{12}$ (5%), and LSW (5%)							
DOC		—	3.1				
DON		0.14	0.27				
FDOM		0.30	0.06				
AOU		0.22	4.1				
DOC	AOU	—	3.1	0%	—	—	0.9184
DOC	DON	0.53	1.8	40%	13	3	0.0027
FDOM	AOU	0.33	0.06	2%	—	—	0.5116
FDOM	DOC	0.21	0.06	0%	—	—	0.9285
Labrador Sea water realm (LSW > 50%; n = 108) SWTs involved: LSW (76%), SPMW (10%), SAIW (5%), ISOW (5%), MW (2%), and LDW (2%)							
DOC		0.42	2.7				
DON		0.15	0.45				
FDOM		0.68	0.06				
AOU		0.68	6.8				
DOC	AOU	0.53	2.4	10%	–0.45	0.09	0.0000
DOC	DON	0.45	2.6	3%	—	—	0.0141
FDOM	AOU	0.76	0.05	13%	0.009	0.002	0.000
FDOM	DOC	0.68	0.06	0%	—	—	0.2400
Dense overflows waters realm (DSOW + ISOW > 50%; n = 15) SWTs involved: ISOW (52%), LSW (27%), DSOW (14%), LDW (4%), and SPMW (3%)							
DOC		0.11	2.7				
DON		0.13	0.47				
FDOM		—	0.03				
AOU		0.99	0.7				
DOC	AOU	0.02	2.7	0%	—	—	0.6931
DOC	DON	0.09	2.7	0%	—	—	0.4176
FDOM	AOU	—	0.03	0%	—	—	0.3839
FDOM	DOC	—	0.03	0%	—	—	0.2853

N_1	N_2	R^2	SD res	% SD reduction	β	SD(β)	p
Lower deep water realm (LDW > 50%; n = 33) SWTs involved: LDW (76%), ISOW (14%), LSW (9%), and MW (1%)							
DOC		—	3.0				
DON		—	0.53				
FDOM		—	0.12				
AOU		0.73	2.2				
DOC	AOU	0.12	3.0	2%	—	—	0.1670
DOC	DON	0.09	2.9	6%	11	5	0.0386
FDOM	AOU	—	0.12	0%	—	—	0.7657
FDOM	DOC	—	0.12	0%	—	—	0.4373

Fig. 1. Chart of the eastern North Atlantic, showing the 91 hydrographic stations occupied during the OVIDE 2002 cruise, aboard R/V *Thalassa*, from 19 June to 11 July 2002. Black dots, stations where DOC, DON, and CDOM measurements were performed at selected depths throughout the entire water column (maximum 15 levels). IAP, Iberian Abyssal Plain.

Fig. 2. Distribution of northeast North Atlantic water masses along the OVIDE 2002 section. Samples with >50% of subtropical thermocline waters ($ENACW_{15}$ + $ENACW_{12}$) subpolar thermocline waters ($ENACW_{12}$ + SPMW); Mediterranean water (MW); Labrador water (LSW); dense overflows waters (DSOW+ISOW); and deep water (LDW) are shown. Solid vertical lines indicate changes of orientation of the section.

Fig. 3. (a) Distributions of nitrate (NO_3) in μmol kg^{-1}; (b) dissolved organic nitrogen (DON) in μmol kg^{-1}; and (c) fluorescence of dissolved organic matter (FDOM) in QSU along the OVIDE 2002 section. Solid vertical lines indicate changes of orientation of the section.

Fig. 4. (a) Archetypical concentrations of dissolved organic carbon($<DOC_i>$) in μmol kg^{-1}; (b) apparent oxygen utilisation ($<AOU_i>$) in μmol kg^{-1}; (c) dissolved organic nitrogen ($<DON>$) in μmol kg^{-1}; (d) C:N ratio of DOM ($<DOC_i>$:$<DON_i>$) in mol C mol N^{-1}; (e) fluorescence of dissolved humic–like substances $<FDOM_i>$ in QSU; and (f) C–specific $FDOM_i$ ($<FDOM_i>$:$<DOC_i>$) in g eq of QS mol of C^{-1}, in the source water types sampled along the OVIDE 2002 section.

Fig. 5. X–Y plots of (a) archetypal dissolved organic carbon ($<DOC_i>$) vs. archetypal apparent oxygen utilization ($<AOU_i>$); (b) $<DOC_i>$ vs. archetypal dissolved organic nitrogen ($<DON_i>$); (c) archetypal C:N ratio of DOM_i ($<DOC_i>$:$<DON_i>$) vs. archetypal pressure ($<Z_i>$); (d) $<DOC_i>$:$<DON_i>$ vs. $<AOU_i>$; (e) archetypal fluorescence of dissolved humic–like substances $<FDOM_i>$ vs. $<DOC_i>$; and (f) $<FDOM_i>$ vs. $<AOU_i>$.

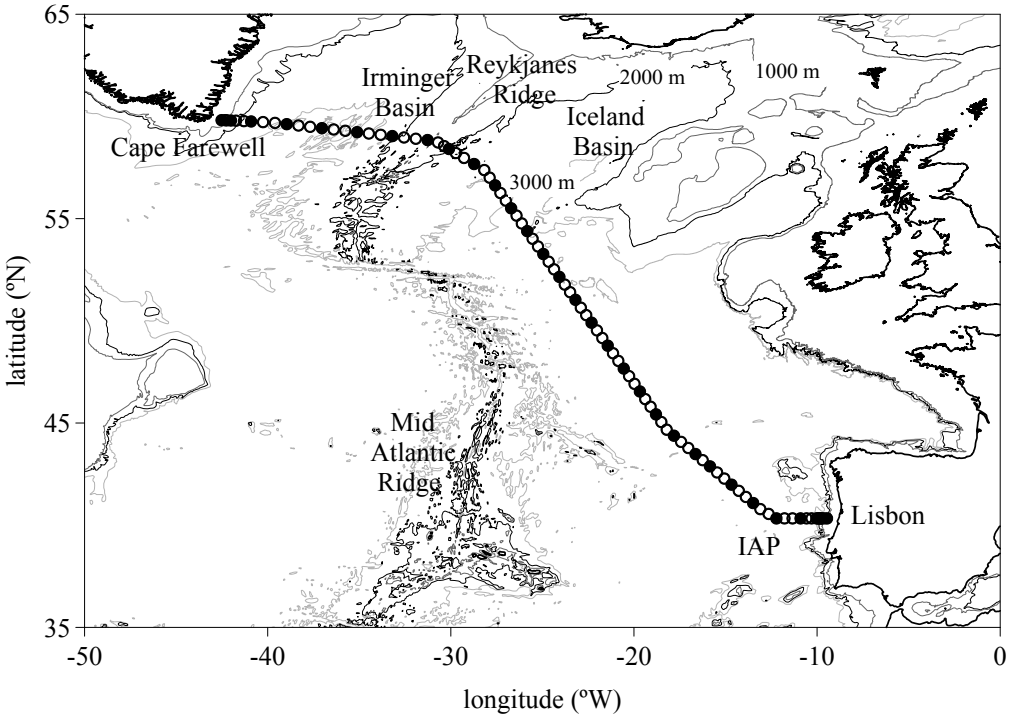

Álvarez–Salgado et al., Fig. 1

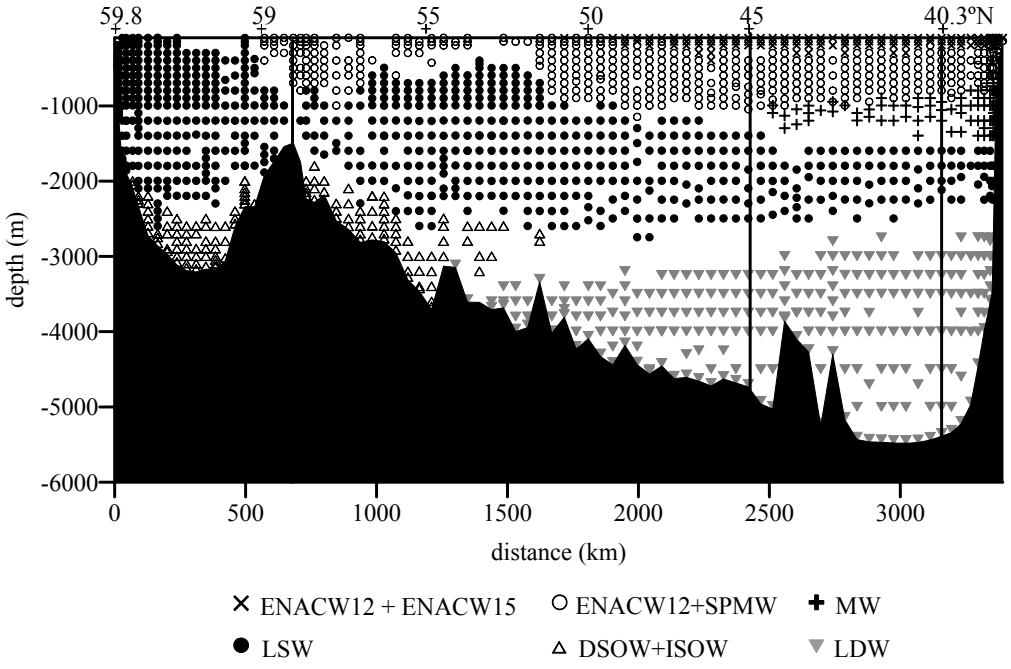

Álvarez–Salgado et al., Fig. 2

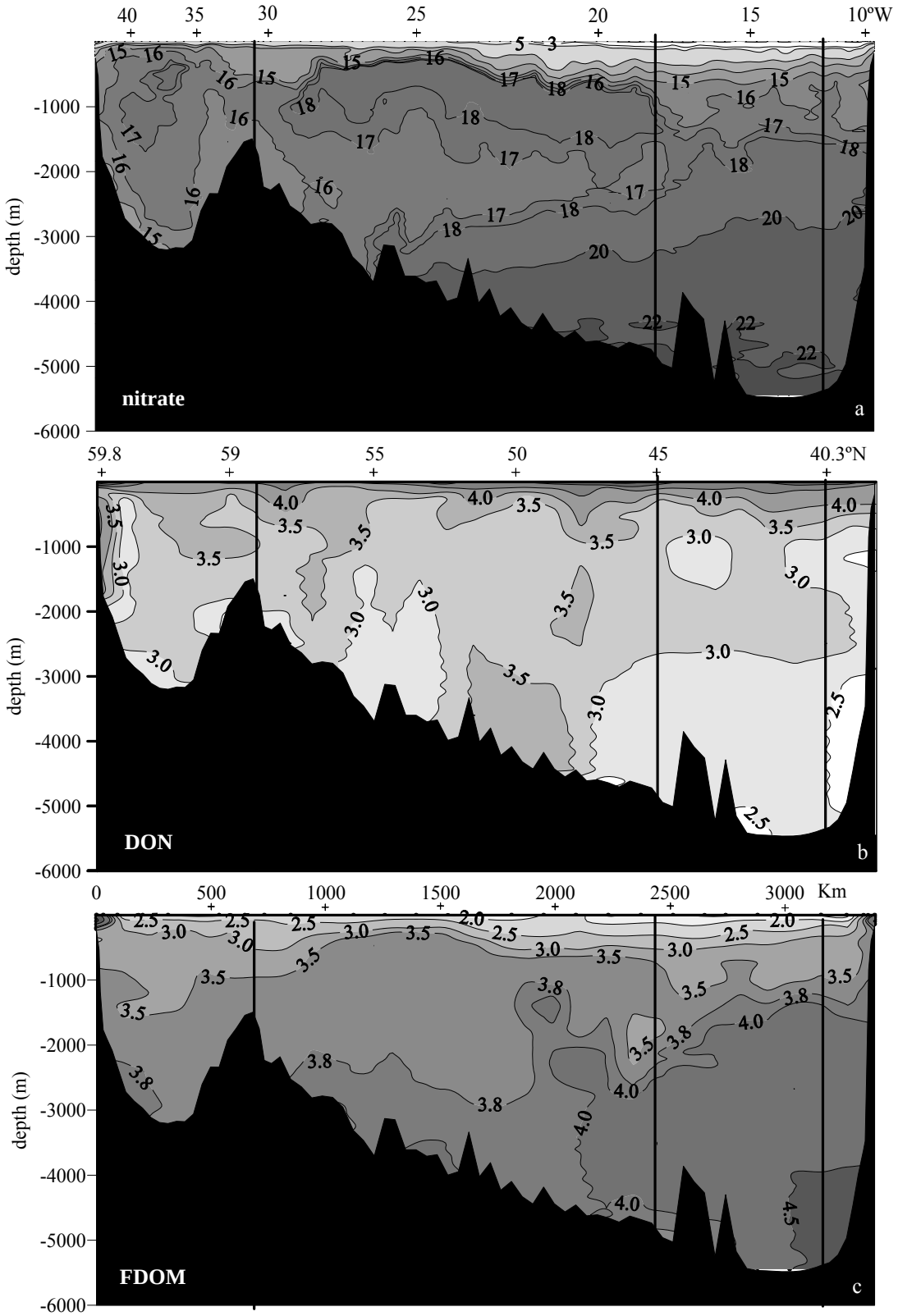

Álvarez–Salgado et al., Fig. 3

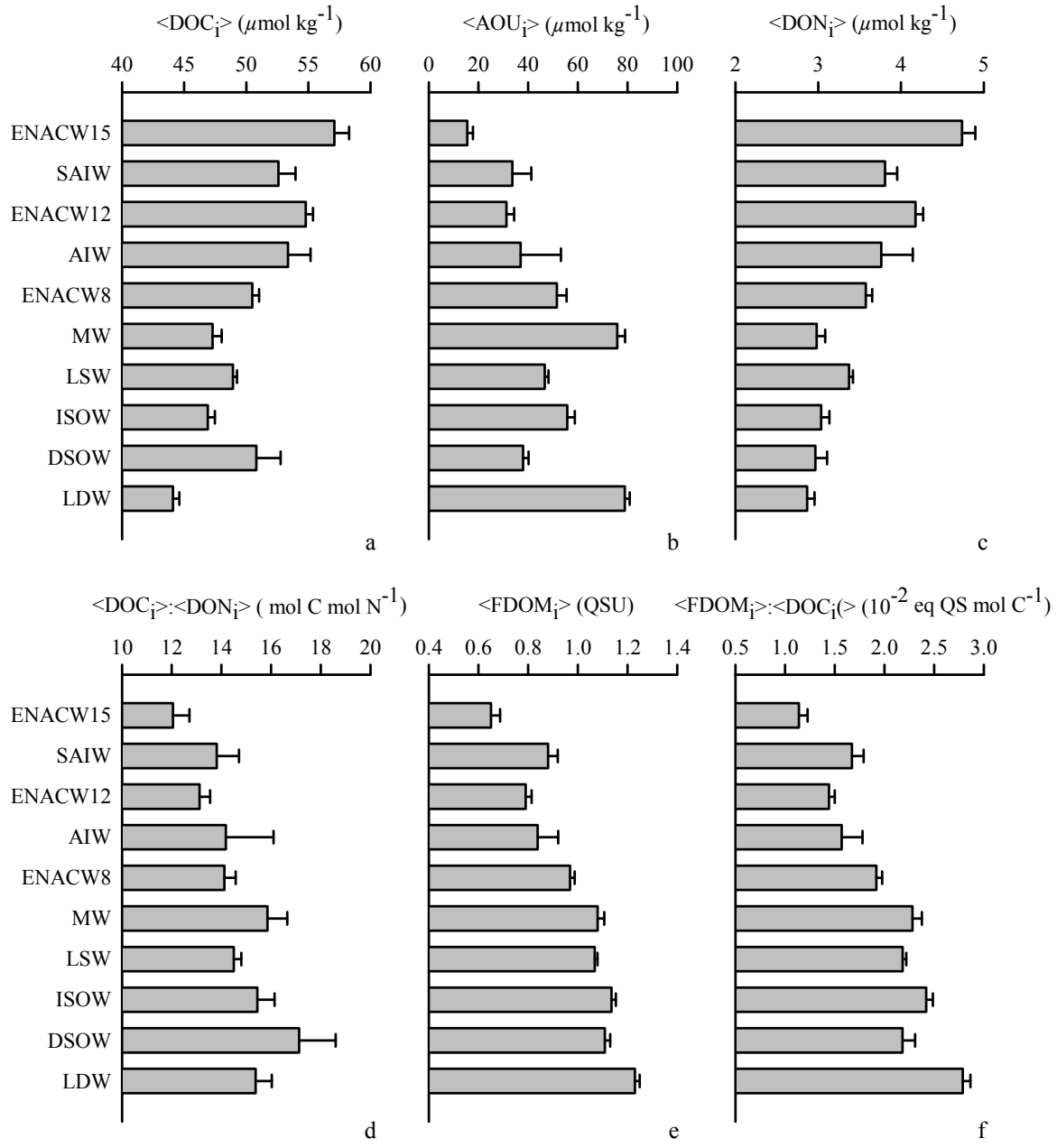

Álvarez–Salgado et al., Fig. 4

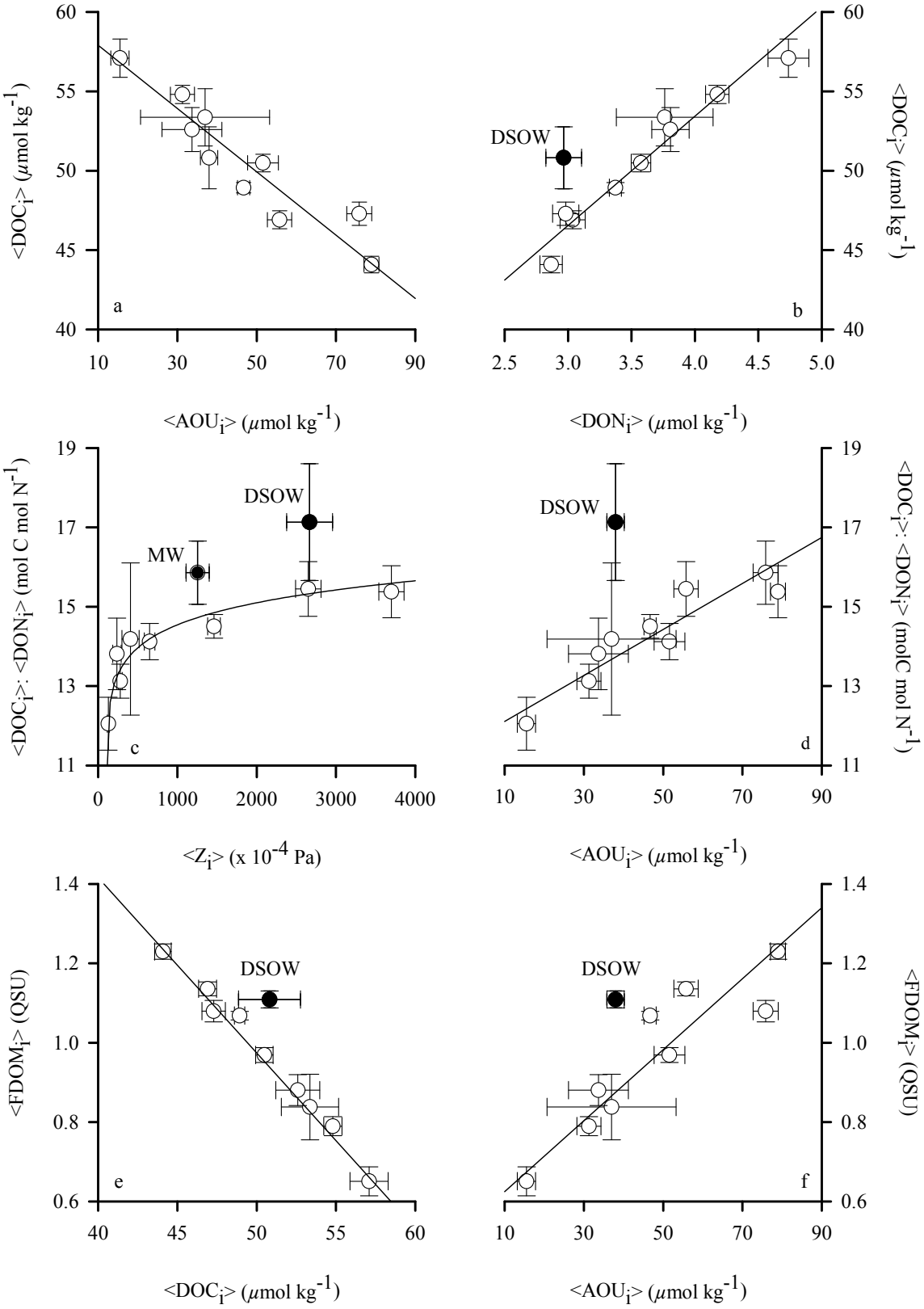

Álvarez–Salgado et al., Fig. 5